Journal of Materials Chemistry A

Bifunctional conjugated polymer photocatalysts for visible light water oxidation and CO_2 reduction: Function- and site-selective hybridisation of Ru(II) complex catalysts

Journal:	*Journal of Materials Chemistry A*
Manuscript ID	TA-ART-06-2024-004014.R1
Article Type:	Paper
Date Submitted by the Author:	16-Aug-2024
Complete List of Authors:	Ishihara, Kotaro; Kyoto University Faculty of Engineering Graduate School of Engineering, Department of Energy and Hydrocarbon Chemistry Nakada, Akinobu; Kyoto University Faculty of Engineering Graduate School of Engineering, Department of Energy and Hydrocarbon Chemistry Suzuki, Hajime; Kyoto University, Tomita, Osamu; Kyoto University, Graduate School of Engineering Nozawa, Shunsuke; High Energy Accelerator Research Organization, Photon Factory Saeki, Akinori; Osaka University, Department of Applied Chemistry, Graduate School of Engineering Abe, Ryu; Kyoto University, Engineering

ARTICLE

Bifunctional conjugated polymer photocatalysts for visible light water oxidation and CO_2 reduction: Function- and site-selective hybridisation of Ru(II) complex catalysts

Received 00th January 20xx,
Accepted 00th January 20xx

DOI: 10.1039/x0xx00000x

Kotaro Ishihara,[a] Akinobu Nakada,*[a,b] Hajime Suzuki,[a] Osamu Tomita,[a] Shunsuke Nozawa,[c] Akinori Saeki [d] and Ryu Abe *[a]

Conjugated polymers have shown potential as photocatalyst materials owing to their molecular design flexibility in tuning their properties, including visible-light absorption. However, most reported conjugated polymers have only a single type of catalytic site and thus exhibit a single photocatalytic function, for example, H_2 evolution, CO_2 reduction, or water oxidation. To achieve artificial photosynthetic reactions, such as CO_2 reduction coupled with water oxidation, it is desirable to construct a strategy for introducing two different catalytic centres for selective oxidation and reduction; these catalysts should be positioned appropriately for photoinduced charge separation in the photocatalyst material. In this study, conjugated polymer photocatalysts were rationally designed for the functional- and site-selective introduction of two-different Ru complex catalysts for water oxidation and CO_2 reduction. A pyrene moiety with condensed aromatic rings blended in a carbazole–bipyridine-based conjugated polymer anchors an isoquinoline ligand of a Ru complex which facilitates water oxidation, whereas the bipyridine moiety selectively hosts another Ru complex for CO_2 reduction. Function- and site-selective hybridisation of the two specific Ru(II) complex catalysts enables the donor–acceptor polymer to act as a bifunctional photocatalyst for visible-light water oxidation and CO_2 reduction.

Introduction

The utilisation of solar energy for molecular conversions, such as CO_2 reduction and H_2 production, has been an important challenge in generating chemical and energy resources that do not depend on fossil resources. The use of water as an electron and proton source is the ultimate way to drive photocatalytic molecular conversion into value-added chemicals. Inorganic semiconductors,[1–3] metal complexes,[4–6] and their hybrid materials[7,8] have been extensively studied as photocatalysts for water oxidation and CO_2 reduction. The use of photocatalyst powder without electrode has been proposed to be a cost-effective way toward practical large-scale operation.[9,10] It is strongly desired to harness visible light that covers approximately half of the sunlight energy for the photocatalytic reactions. However, visible-light-driven CO_2 reduction using water as an electron/proton source has hardly been achieved except for a few semiconductor photocatalysts and their hybridised systems with metal complexes, where stable inorganic semiconductors are used for water oxidation.[11–13]

Recently, conjugated polymers have attracted significant attention as new and promising heterogeneous photocatalyst materials.[14–16] The conjugated polymers exhibit visible-light absorption owing to their expanded π-conjugation with flexible molecular designability for engineering HOMO–LUMO energies.[17] In addition, molecular-based materials, including conjugated polymers, have opportunities to introduce specific anchoring moieties that selectively bind catalyst molecules, such as metal complexes. Incorporation of a molecular unit that acts as a ligand in the polymer is one of the simplest ways to site-selectively introduce a metal complex catalyst.[18,19] We recently reported linear conjugated polymers with a bipyridine (bpy) unit that acts as a ligand anchoring the Ru(II) carbonyl complex catalyst for photocatalytic CO_2 reduction.[20] The introduction of an electron-donating carbazole skeleton resulted in selective LUMO localisation on the bpy ligand which coordinates to the Ru(II) complex. Hence, the molecular design enabled effective trapping of the photoexcited electrons at the Ru(II) catalyst moiety, engaging in significantly more efficient CO_2 reduction than its phenyl and benzothiadiazole counterparts. However, the reported conjugated polymer photocatalysts, including this system,[20] can only drive the CO_2 reduction half-reaction with a sacrificial electron donor. Therefore, it is important to introduce another catalytic site for water oxidation into the polymer photocatalysts at a different

[a] Department of Energy and Hydrocarbon Chemistry, Graduate School of Engineering, Kyoto University, Nishikyo-ku, Kyoto 615-8510, Japan. E-mail: nakada@scl.kyoto-u.ac.jp (AN), ryu-abe@scl.kyoto-u.ac.jp (RA)
[b] Precursory Research for Embryonic Science and Technology (PRESTO), Japan Science and Technology Agency (JST), 4-1-8 Honcho, Kawaguchi, Saitama 332-0012, Japan.
[c] Photon Factory (PF), Institute of Materials Structure Science (IMSS), High Energy Accelerator Research Organization (KEK), Tsukuba, Ibaraki 305-0801, Japan.
[d] Department of Applied Chemistry, Graduate School of Engineering, Osaka University, 2-1 Yamadaoka, Suita, Osaka 565-0871, Japan.
† Footnotes relating to the title and/or authors should appear here.
Electronic Supplementary Information (ESI) available: [details of any supplementary information available should be included here]. See DOI: 10.1039/x0xx00000x

position where photogenerated holes are favourably located, toward coupling CO_2 reduction and water oxidation.

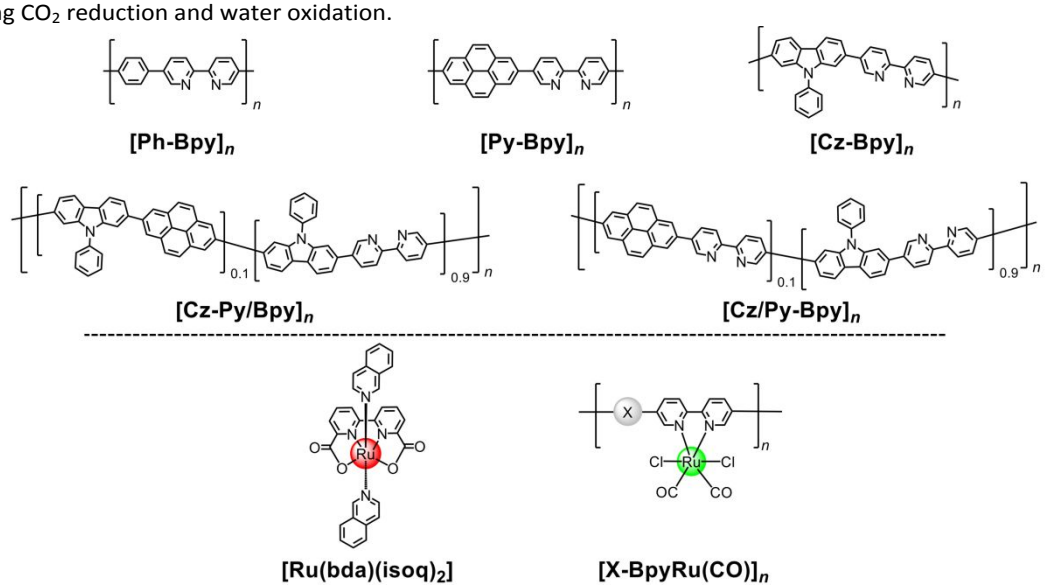

Fig. 1 Molecular structures and abbreviations of conjugated polymers and Ru(II) complex catalyst moieties used in this study.

With the aid of cocatalyst species, some conjugated polymer photocatalysts have been reported to facilitate water oxidation,[21–23] although the number of reports is significantly smaller than that for CO_2 reduction.[24] Co-,[21] Ir-,[22] and Ru-based[23] nanoparticulate species have been mainly employed as cocatalysts in polymer photocatalysts for water oxidation. In these studies, the choice of cocatalyst species was inspired by the research on inorganic semiconductor photocatalysts.[12,25] However, the relatively low thermal stability of organic polymer materials narrows the range of selection for the loading method of cocatalysts because thermal treatment is one of the common ways for loading nanoparticulate cocatalysts on inorganic photocatalysts.

Molecular metal complexes are also a promising candidate for water oxidation. In particular, Ru complexes with a bipyridine-6,6'-dicarboxylato (bda) ligand are known to exhibit extremely high catalytic activity for water oxidation in the presence of an electrochemical applied potential[26] or a chemical oxidant.[27] The Ru(bda) complex catalysts have also been used for photocatalytic application in a homogeneous solution system with a $[Ru(bpy)_3]^{2+}$ type photosensitizer.[28,29] Although modification of the Ru(bda) complex on an electrode surface for photoelectrochemical water oxidation has been demonstrated,[30] heterogeneous photocatalysts hybridised with Ru(bda) complex catalyst have hardly been reported. Condensed aromatic materials such as graphene are known to host π-conjugated molecules through π–π interactions.[31] For instance, a graphene electrode, hybridised with a Co phthalocyanine complex through π–π interactions, has shown high efficiency and robust CO_2 electroreduction.[32] Therefore, we expect that conjugated polymer photocatalysts act as potential platforms for the simple and mild hybridisation of molecular catalysts, such as Ru(bda), by introducing molecular interactions.

In this study, we developed conjugated polymer photocatalysts with a host backbone for the hybridisation of a Ru(bda) catalyst for visible-light water oxidation. Some types of conjugated building blocks were employed as the host moiety to recognise a Ru(bda) catalyst with a condensed isoquinoline (isoq) ligand ($[Ru(bda)(isoq)_2]$, Fig. 1). Through site-selective introduction of the host moiety, our aim was to modify $[Ru(bda)(isoq)_2]$ at an appropriate position of the conjugated polymer where photogenerated holes are favourably located to effectively be utilized for the water oxidation catalysis. We also demonstrated that the same conjugated polymer bifunctionally facilitates visible-light CO_2 reduction in aqueous solution through selective coordination of a different Ru-complex catalyst at the bipyridine ligand unit (Fig. 1).

Results and discussion

Effects of conjugated skeleton on light absorption, HOMO–LUMO potentials, and modification of Ru complex catalysts for water oxidation

Conjugated polymers **[X-Bpy]*n*** with different conjugated skeletons (Fig. 1; X = phenyl (Ph), pyrene (Py), and carbazole (Cz)) were synthesised using Suzuki–Miyaura cross-coupling reactions between dibromobipyridine and boronic esters corresponding to the X units. The matrix-assisted laser desorption/ionization time-of-flight mass spectrometry (MALDI-TOF-MS) of the obtained materials exhibited repeated peaks with interpeak *m/z* differences corresponding to the **X-Bpy** unit (Fig. S1), indicating the formation of alternating [**X-Bpy**] networks. The maximum numbers of connected units detected in the MALDI-TOF-MS spectra were 32, 16, and 16 for **[Ph-bpy]*n***, **[Py-Bpy]*n***, and **[Cz-Bpy]*n***, respectively. The scanning electron microscope (SEM) images showed the aggregated

structures of **[Ph-Bpy]$_n$**, **[Py-Bpy]$_n$**, and **[Cz-Bpy]$_n$**, which are several micrometres in size (Fig. S2).

The polymerisation of the colourless monomers afforded green-to-yellow powders. **[X-Bpy]$_n$** (X = Ph, Py, or Cz) exhibited visible light absorption, of which the absorption edges were slightly red-shifted in the following order: X = Ph (447 nm) < Py (453 nm) < Cz (457 nm) (Fig. 2a). The HOMO–LUMO levels, derived from their HOMO–LUMO energy gaps (E_g) and ionisation energies measured by photoelectron yield spectroscopy (PYS), are summarised in Fig. 2b. **[Py-Bpy]$_n$** exhibited a similar HOMO–LUMO gap with slightly stabilised HOMO–LUMO levels as **[Ph-Bpy]$_n$**. In the case of **[Cz-Bpy]$_n$**, an upward shift in the HOMO energy was observed owing to the electron-donating nature of carbazole.[20] Although different X moieties reasonably change the HOMO–LUMO energies, the differences are not significantly large within the range of 0.1–0.2 eV. More importantly, the electrocatalytic onset potential of [Ru(bda)(isoq)$_2$] for water oxidation was reported to be 1.04 V vs. SHE at pH 7,[33] which is approximately 200–400 mV more negative than the HOMO levels of the polymers (Fig. 2b). This implies that all the polymers have a thermodynamic driving force to proceed with the water oxidation reaction using their photogenerated holes.

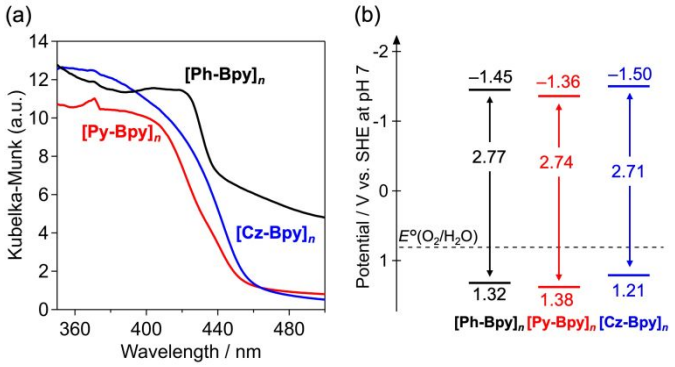

Fig. 2 (a) UV–visible diffuse reflectance spectra of the polymer photocatalysts and (b) HOMO–LUMO potentials of **[Ph-Bpy]$_n$**, **[Py-Bpy]$_n$**, and **[Cz-Bpy]$_n$**.

Hybridisation of [Ru(bda)(isoq)$_2$] with the polymers was performed by stirring **[X-Bpy]$_n$** in a MeCN-H_2O (9:1, *v/v*) solution of [Ru(bda)(isoq)$_2$]. The adsorption isotherms indicate Langmuir-type adsorption of [Ru(bda)(isoq)$_2$] with an equilibrium constant of 4.1 × 10^{-3} M^{-1} for **[Py-Bpy]$_n$** (Fig. 3a). **[Py-Bpy]$_n$** exhibited saturation adsorption of 68.0 μmol/mmol, which is significantly larger than **[Ph-Bpy]$_n$** (6.9 μmol/mmol) and **[Cz-Bpy]$_n$** (19.6 μmol/mmol). Hence, the pyrene unit was assumed to affect the interaction between the polymer and [Ru(bda)(isoq)$_2$]. The diffuse reflectance spectra (DRS) of the polymer exhibited only slight changes before and after the adsorption of [Ru(bda)(isoq)$_2$] (Fig. S3). In contrast, the Ru-K edge X-ray absorption near edge structure (XANES) spectrum of the obtained [Ru(bda)(isoq)$_2$]/**[Py-Bpy]$_n$** hybrid clearly showed the signature features of the original complex [Ru(bda)(isoq)$_2$] (Fig. S4), indicating that [Ru(bda)(isoq)$_2$] maintains its coordination structure after hybridisation.

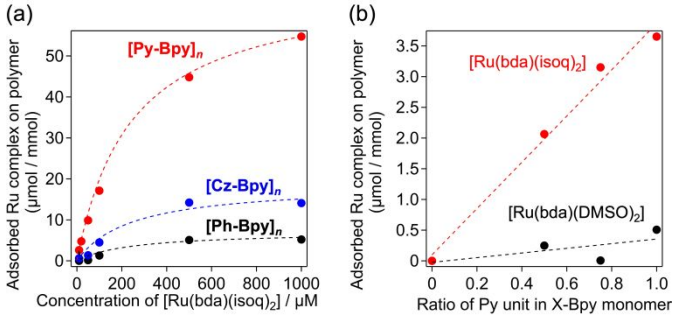

Fig. 3 (a) Adsorption isotherms of [Ru(bda)(isoq)$_2$] on **[X-Bpy]$_n$** particles in an aqueous MeCN solution (10 vol%). (b) Adsorbed amounts of [Ru(bda)L_2] complexes (10 μM; L = isoq or DMSO) against the molar ratio of pyrene moiety in the conjugated polymers (see Fig. S5 for their molecular structures).

The impact of the pyrene moiety on hybridisation was further investigated by introducing pyrene/bipyridine-based polymers with different pyrene contents (refer Figs. S5 for molecular structures). The amount of adsorbed [Ru(bda)(isoq)$_2$] increased almost proportionally with the molecular ratio of the Py moiety in the polymer (red plots in Fig. 3b). In contrast, the adsorption was negligible for the [Ru(bda)(DMSO)$_2$] complex instead of [Ru(bda)(isoq)$_2$], regardless of the Py content in the polymer (black plots in Fig. 3b). This clearly indicates the importance of isoquinoline ligands in adsorption. From these observations, we can conclude that the pyrene moiety in the polymer plays an important role as a recognition site for the hybridisation of the [Ru(bda)(isoq)$_2$] complex through π–π interactions with the isoquinoline ligand.

Photocatalytic water oxidation by conjugated polymers hybridised with a [Ru(bda)(isoq)$_2$] catalyst

Photocatalytic water oxidation was performed in an aqueous solution containing $Na_2S_2O_8$ (10 mM). Although **[Py-Bpy]$_n$** itself did not show photocatalytic O_2 evolution activity upon visible light irradiation (λ > 400 nm), hybridisation of the [Ru(bda)(isoq)$_2$] complex with **[Py-Bpy]$_n$** triggered O_2 evolution (Table 1, entries 1 and 2). No activity was observed when [Ru(bda)(isoq)$_2$] was used without **[Py-Bpy]$_n$** (Table 1, entry 3). In the absence of $Na_2S_2O_8$ or photoirradiation, the [Ru(bda)(isoq)$_2$]-modified **[Py-Bpy]$_n$** ([Ru(bda)(isoq)$_2$]/**[Py-Bpy]$_n$**) did not generate O_2 (Table 1, entries 4 and 5). Hence, this reaction represents photocatalytic water oxidation using $Na_2S_2O_8$ as an electron acceptor, driven by a hybrid of **[Py-Bpy]$_n$** and [Ru(bda)(isoq)$_2$].

Table 1 Photocatalytic O_2 evolution under various conditions.[a]

Entry	Polymer	[Ru(bda)(isoq)$_2$]	$Na_2S_2O_8$	Light	Amount of O_2 evolved / nmol
1	**[Py-Bpy]$_n$**	yes	yes	yes	170
2	**[Py-Bpy]$_n$**	no	yes	yes	N.D.
3	none	yes	yes	yes	N.D.
4	**[Py-Bpy]$_n$**	yes	no	yes	N.D.
5	**[Py-Bpy]$_n$**	yes	yes	no	N.D.
6	**[Cz-Bpy]$_n$**	yes	yes	yes	560
7	**[Ph-Bpy]$_n$**	yes	yes	yes	N.D.

[a] Standard conditions: Photocatalyst powder (50 mg), dispersed in a boric acid buffer (20 mM, pH 7.0, adjusted with NaOH) solution (50 mL) containing $Na_2S_2O_8$ (10 mM), was irradiated at λ > 400 nm for 2 h under an Ar atmosphere.

The O_2 evolution activity of the [Ru(bda)(isoq)$_2$]-modified hybrid photocatalyst was strongly dependent on the type of X moiety in **[X-Bpy]$_n$**. The hybrid with **[Cz-Bpy]$_n$** exhibited 3.3 times higher O_2 evolution rate than that of **[Py-Bpy]$_n$**, whereas no activity was observed for [Ru(bda)(isoq)$_2$]/**[Ph-Bpy]$_n$** (Table 1, entries 6 and 7). Significantly lower amount of [Ru(bda)(isoq)$_2$] hybridised with **[Ph-Bpy]$_n$** compared to **[Py-Bpy]$_n$** (see Fig. 3a) is probably the reason for the negligible activity of [Ru(bda)(isoq)$_2$]/**[Ph-Bpy]$_n$**. However, the higher activity of **[Cz-Bpy]$_n$** compared to **[Py-Bpy]$_n$** cannot be simply explained by the amounts of [Ru(bda)(isoq)$_2$] hybridised, considering that **[Cz-Bpy]$_n$** has significantly lower adsorption capability compared **[Py-Bpy]$_n$**. Molecular orbital calculations of the model monomer unit indicated a donor–acceptor nature of **[Cz-Bpy]$_n$**,[20] whereas both HOMO and LUMO were localised on the pyrene moiety in the case of **[Py-Bpy]$_n$** (Fig. S6). It has been reported that introducing a donor–acceptor structure in conjugated polymers facilitates the separation of photoexcited charges trapped as excitons.[34,35] This implies that the higher activity of **[Cz-Bpy]$_n$** is due to its donor–acceptor nature, despite the smaller amount (approximately by 7 times) of the modified Ru-complex catalyst.

To incorporate the superior features of **[Py-Bpy]$_n$** and **[Cz-Bpy]$_n$**, that is, good hybridisation capability and donor–acceptor nature, Py/Cz-mixed polymers were developed. **[Cz-Py/Bpy]$_n$** and **[Cz/Py-Bpy]$_n$**, in which the Py moiety is located next to the Cz and Bpy, respectively (Fig. 1), were synthesised via Suzuki–Miyaura cross-coupling reactions using appropriate building blocks having bromo and boronic ester groups. The Py molar ratio in the building blocks was fixed at 10% (mole ratio) based on the precursor used. The UV–visible absorption and HOMO–LUMO levels were almost unchanged compared to those of **[Cz-Py/Bpy]$_n$**, **[Cz/Py-Bpy]$_n$**, and **[Cz-Bpy]$_n$** (Fig. S7). Importantly, the introduction of only 10% Py moiety obviously enhanced the capability for adsorption of [Ru(bda)(isoq)$_2$] (50 μM in MeCN aq.) by twice for **[Cz-Py/Bpy]$_n$** (3.0 μmol/mmol) and four times for **[Cz/Py-Bpy]$_n$** (5.6 μmol/mmol), compared to that of **[Cz-Bpy]$_n$** (1.4 μmol/mmol).

[Cz-Py/Bpy]$_n$ and **[Cz/Py-Bpy]$_n$** photocatalysed O_2 evolution with the aid of [Ru(bda)(isoq)$_2$] at rates 3.3 and 1.9 μmol h^{-1}, which are approximately 11 and 6 times higher than **[Cz-Bpy]$_n$**, respectively (Fig. 4a). On the other hand, a Py/Ph-mixed polymer **[Ph-Py/Bpy]$_n$** was not effective (0.1 μmol h^{-1}). Therefore, the improved photocatalytic activities should arise from synergy of pyrene anchor moiety and donor-acceptor characters in **[Cz-Py/Bpy]$_n$** and **[Cz/Py-Bpy]$_n$** because their light absorption and HOMO–LUMO levels are similar to **[Cz-Bpy]$_n$**. Importantly, **[Cz-Py/Bpy]$_n$** exhibited higher activity than its iso-structure **[Cz/Py-Bpy]$_n$**, suggesting the importance of pyrene unit location to maximize water oxidation activity of hybridized [Ru(bda)(isoq)$_2$] catalyst (refer their chemical structure in Fig. 1). The turnover number for O_2 formation reached 19.3 based on [Ru(bda)(isoq)$_2$] in the hybrid with **[Cz-Py/Bpy]$_n$**. ATR-IR spectra derived from polymer backbone of **[Cz-Py/Bpy]$_n$** were almost unchanged before and after photocatalytic reaction (Fig. S8). The wavelength dependency of photocatalytic O_2 evolution activities clearly showed the visible light absorption of **[Cz-Py/Bpy]$_n$** is effectively utilized for water oxidation (Fig. 4b). The quantum efficiency of O_2 evolution was 0.07% at 430 nm by using [Ru(bda)(isoq)$_2$]/**[Cz-Py/Bpy]$_n$**.

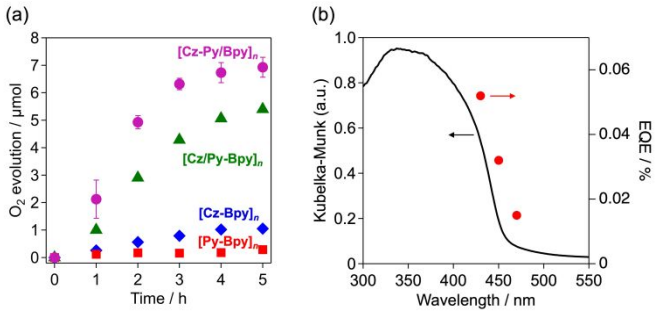

Fig. 4 (a) Time courses of O_2 evolution over [Ru(bda)(isoq)$_2$]–modified **[Py–Bpy]$_n$**, **[Cz–Bpy]$_n$**, **[Cz-Py/Bpy]$_n$**, or **[Cz/Py-Bpy]$_n$** hybrid (50 mg) in a 10 mM $Na_2S_2O_8$ aqueous solution in boric acid buffer (20 mM, pH 7.0 adjusted with NaOH, 50 mL) under visible light (λ > 400 nm). (b) Action spectra of external quantum efficiency (EQE) for O_2 evolution by [Ru(bda)(isoq)$_2$]/**[Cz-Py/Bpy]**.

To gain further insights into the photoinduced charge transfer behaviour, time-resolved spectroscopy and photoelectrochemical measurements were performed. Fig. 5a shows the transient conductivities of **[Cz-Py/Bpy]$_n$** with and without modification with [Ru(bda)(isoq)$_2$]. The photoconductivity values $\phi\Sigma\mu$, where ϕ is the quantum efficiency of charge carrier generation and $\Sigma\mu$ is the sum of photogenerated carrier mobilities, were increased within the instrumental time resolution (~ 10^{-7} s) and then gradually decreased due to charge recombination and/or trapping. The transient photoconductivity signals of **[Cz-Py/Bpy]$_n$** tended to decrease with an increase in the amount of [Ru(bda)(isoq)$_2$] hybridised, which corresponded to an increase in the photocatalytic O_2 evolution rate (Fig. 5b). Considering the oxidation potential of $Ru^{III/II}$ in [Ru(bda)(isoq)$_2$] (E_{ox} = 0.63 V vs. SHE[26]), the decreased photoconductivity is likely owing to the hole transfer from **[Cz-Py/Bpy]$_n$** (E_{HOMO} = 1.27 V; Fig. S7).

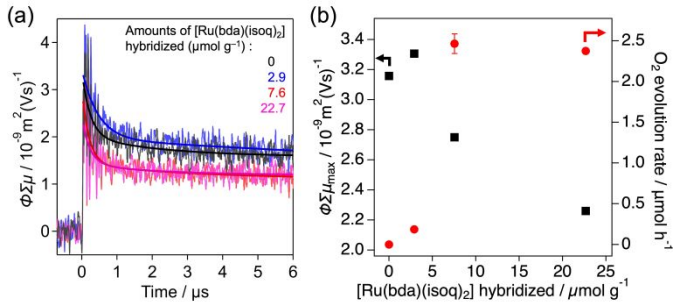

Fig. 5 (a) Transient photoconductivities and its fitting using a biexponential function ($A_1\exp(-k_1t) + A_2\exp(-k_2t)$) of **[Cz-Py/Bpy]$_n$** with different amounts of [Ru(bda)(isoq)$_2$] hybridised. (b) Dependency of transient conductivities at t = 0 and O_2 evolution rates on the amount of [Ru(bda)(isoq)$_2$] hybridised.

Fig. 6 shows the time courses of the photocurrent from the **[Cz-Bpy]$_n$**, **[Cz-Py/Bpy]$_n$**, and **[Cz/Py-Bpy]$_n$** electrodes with and without the modification of [Ru(bda)(isoq)$_2$] upon visible-light irradiation (λ > 400 nm) at an applied potential of 1.0 V (vs. Ag/AgCl). In the absence of [Ru(bda)(isoq)$_2$], all three polymers exhibited a photoanodic current (black lines) attributable to the photoinduced electron injection from the polymer to the electrode. Hybridising them with [Ru(bda)(isoq)$_2$] increased the photoanodic current (red lines). The total numbers of passed electrons increased by [Ru(bda)(isoq)$_2$] modification were 7.8, 19.7, and 10.1 nmol for **[Cz-Bpy]$_n$**, **[Cz-Py/Bpy]$_n$**, and **[Cz/Py-Bpy]$_n$**, respectively, upon 60 min of photoirradiation. The increased numbers of electrons were more than 1000 times higher than the moles of loaded [Ru(bda)(isoq)$_2$] ($0.3–1.4\times10^{-2}$ nmol), supporting the progress of catalytic water oxidation by [Ru(bda)(isoq)$_2$] using photogenerated holes on the polymer electrode. The magnitudes of increased photocurrent at the steady state by hybridisation of [Ru(bda)(isoq)$_2$] were in the following order: **[Cz-Bpy]$_n$** < **[Cz/Py-Bpy]$_n$** < **[Cz-Py/Bpy]$_n$**. From the results of time-resolved spectroscopies and photoelectrochemical measurements, we can conclude that the [Ru(bda)(isoq)$_2$] catalyst could utilise photogenerated holes for water oxidation, most effectively on **[Cz-Py/Bpy]$_n$** through hybridization on the pyrene unit next to the carbazole donor moiety. The molecular orbital distributions calculated for the corresponding monomers showed a clear HOMO–LUMO separation from the Py anchor to the Cz-Bpy skeleton in **Cz-Py/Bpy** (Fig. 7a). In contrast, the HOMO was located on the Cz unit that was far from the Py anchor, whereas the LUMO was located on the Bpy unit in **Cz/Py-Bpy** (Fig. 7b). Hence, the [Ru(bda)(isoq)$_2$] catalyst modified on the pyrene unit in **[Cz-Py/Bpy]$_n$** was more effectively activated by photogenerated holes (Fig. 7), leading to better photocatalytic water oxidation activity than **[Cz/Py-Bpy]$_n$** (Fig. 4a).

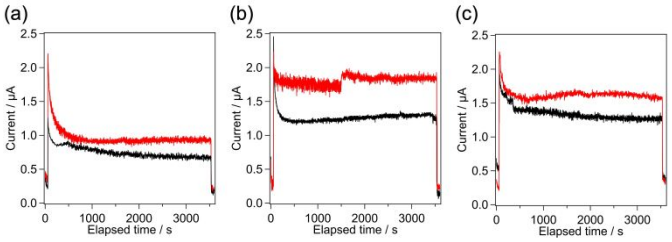

Fig. 6 Time courses of photocurrents through the (a) **[Cz-Bpy]$_n$**, (b) **[Cz-Py/Bpy]$_n$**, and (c) **[Cz/Py-Bpy]$_n$** electrodes with (red lines) and without (black lines) modification of [Ru(bda)(isoq)$_2$] upon visible-light irradiation (λ > 400 nm) at an applied potential of 1.0 V (vs. Ag/AgCl).

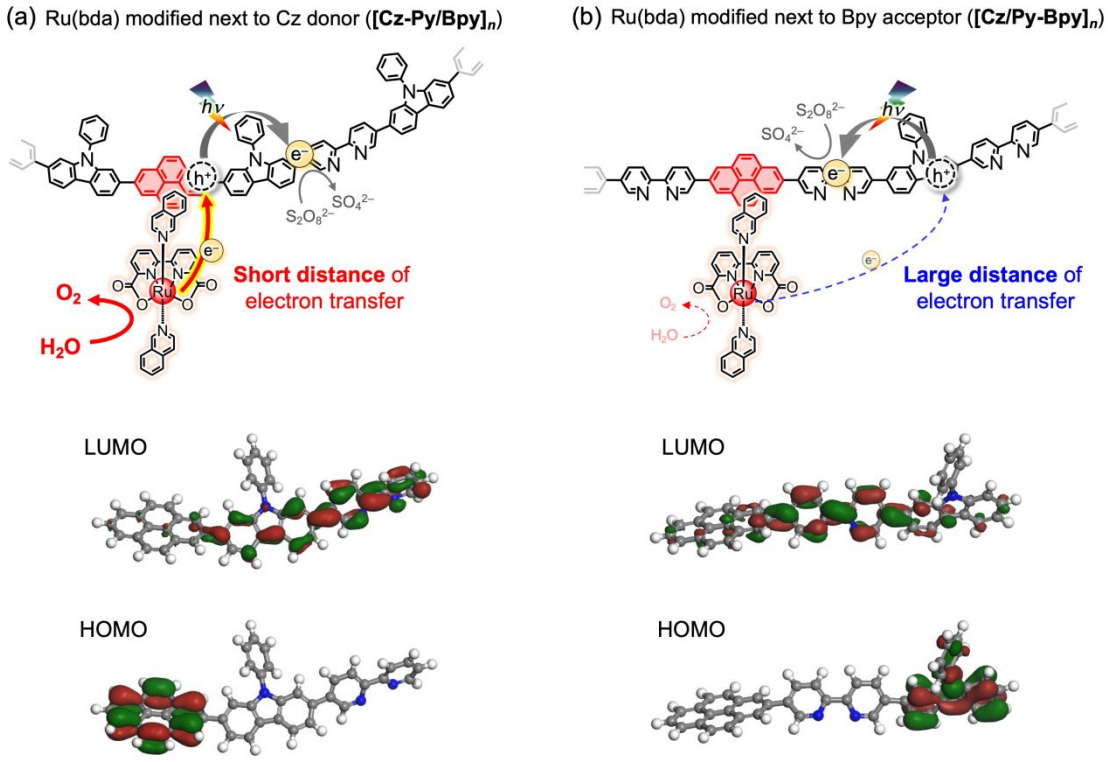

Fig. 7 Assumed mechanism for O_2 evolution over [Ru(bda)(isoq)$_2$]-modified (a) **[Cz-Py/Bpy]$_n$** and (b) **[Cz/Py-Bpy]$_n$**.

Ruthenium-based nanoparticles such as RuO_x species, which are prepared from a precursor such as $RuCl_3$ via heating[36] or non-thermal adsorption processes,[37] are known to act as co-catalysts that boost water oxidation on the surface of inorganic semiconductor photocatalysts. Hence, the possibility that the hybridised [Ru(bda)(isoq)$_2$] was converted to the conventional RuO_x cocatalyst was investigated by means of extended X-ray absorption fine structure (EXAFS). Although the molecular structure of [Ru(bda)(isoq)$_2$] hybridised on **[Cz-Py/Bpy]$_n$** changed during photocatalysis, the EXAFS spectra indicated the formation of trinuclear Ru complex species[38] bridged by the μ-oxo ligand (Fig. S9). In addition, visible-light irradiation of a mixture of **[Cz-Py/Bpy]$_n$** and $RuCl_3$ did not produce O_2 in the presence of the $Na_2S_2O_8$ electron acceptor (Fig. S10). This indicates the importance of introducing a structurally defined molecular catalyst into the designed polymer photocatalyst for visible-light water oxidation.

Photocatalytic CO_2 reduction by conjugated polymers bearing a Ru(II) carbonyl complex

The potential of the conjugated polymers developed in this study for CO_2 reduction were also evaluated in an aqueous solution. According to our previous report,[20] the Ru carbonyl complex moiety was introduced by coordination to the bipyridine unit in the polymers (**[X-BpyRu(CO)]$_n$**). **[Cz-Py/BpyRu(CO)]$_n$** and **[Cz-BpyRu(CO)]$_n$** were found to facilitate photocatalytic CO_2 reduction giving formate as the main product even in aqueous solution with the aid of sodium ascorbate as a sacrificial electron donor (Fig. 8). The EQE for formate formation was estimated as 0.02% at 430 nm. In contrast, CO_2 reduction did not proceed on **[Cz-Py/BpyRu(CO)]$_n$** in the absence of CO_2, light, or sodium ascorbate (Table S1, entries 1-4), indicating that the CO_2 reduction was driven by visible light using ascorbate as an electron donor. The conjugated polymer itself (**[Cz-Py/Bpy]$_n$**) generated negligible products (Table S1, entry 5), suggesting that the Ru(CO) complex moiety catalyse CO_2 reduction with similar selectivity as reported for Ru(bpy)(CO)$_2$Cl$_2$-type complex catalyst in aqueous solution.[39]

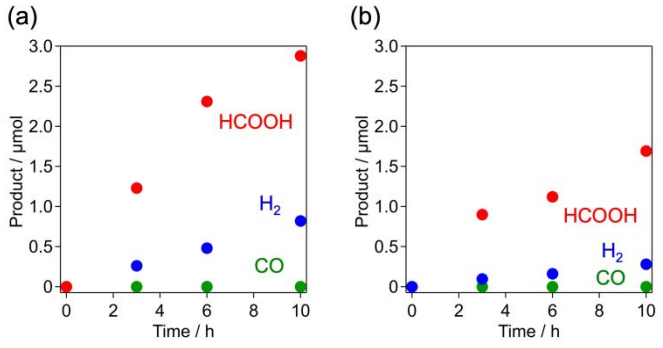

Fig. 8 Time courses of the formation of formate, CO, and H_2 over (a) **[Cz-Py/BpyRu(CO)]$_n$** and (b) **[Cz-BpyRu(CO)]$_n$** in an aqueous solution containing sodium ascorbate (10 mM) and Na_2CO_3 (50 mM) upon visible-light irradiation (λ > 400 nm).

Interestingly, **[Cz-Py/BpyRu(CO)]$_n$** exhibited better CO_2 reduction activity than previously reported **[Cz-BpyRu(CO)]$_n$**. Transient photoconductivity measurements indicated that **[Cz-Py/Bpy]$_n$** shows larger photoconductivity than **[Cz-Bpy]$_n$** (Fig. S11), possibly due to the expanded charge separation in presence of pyrene moiety (Fig 7a). The superior photoconductivity of **[Cz-Py/Bpy]$_n$** skeleton may account for the better transport of photoexcited electrons to the Ru-complex catalyst moiety, resulting in enhanced photocatalytic activity for CO_2 reduction.

It should be noted that **[Cz-Py/Bpy]$_n$** acted as a bifunctional photocatalyst for water oxidation and CO_2 reduction in aqueous solution, by site-selectively hybridising [Ru(bda)(isoq)$_2$] and Ru(CO) complex moieties, respectively. To the best of our knowledge, this is an extremely rare example of bifunctional conjugated polymer photocatalyst workable for water oxidation and CO_2 reduction in aqueous solution as has been reported only for g-C_3N_4[40,41] (Table S2). Because **[Cz-Py/BpyRu(CO)]$_n$** was effective for CO_2 reduction in aqueous solutions, we attempted to co-incorporate two different Ru complex catalysts (i.e. [Ru(bda)(isoq)$_2$] and **Ru(CO)**) to achieve CO_2 reduction using water as an electron donor. However, the multi-catalyst hybrid [Ru(bda)(isoq)$_2$]/**[Cz-Py/BpyRu(CO)]$_n$** exhibited negligible photocatalytic activity in pure water; in particular, no formate was detected despite the formation of small amounts of H_2 and CO (Fig. S12). The hybrid was found to photocatalyse formate oxidation (Fig. S13), which competes with water oxidation. The re-oxidation of formate could be one of the possible reasons for the negligible activity of CO_2 reduction in pure water. Further catalyst design to suppress back-chemical reactions is an important challenge for successful coupling of CO_2 reduction and water oxidation.

Conclusions

In this study, we demonstrate the function-selective modification of two different Ru(II) complex catalysts for water oxidation and CO_2 reduction by introducing appropriate molecular units into conjugated polymers. A pyrene moiety, which has condensed aromatic rings in the conjugated polymers, was found to act as an anchor for the [Ru(bda)(isoq)$_2$] complex catalyst through recognition of the isoquinoline ligand. Introduction of a pyrene moiety next to a carbazole (Cz) donor unit in a carbazole–bipyridine-based polymer enabled the hybridisation of the [Ru(bda)(isoq)$_2$] catalyst in the vicinity of favourably distributed photogenerated holes (on Py). The manipulation of photogenerated holes and site-selective introduction of catalyst led to effective visible-light activation of water oxidation catalysis. In addition, the pyrene-incorporated polymer hybridised with another Ru(II) complex catalyst in bipyridine ligand moiety, **[Cz-Py/BpyRu(CO)]$_n$**, facilitated visible light CO_2 reduction even in an aqueous media. The introduction of pyrene expanded donor–acceptor charge separation, leading to the better photoconductivity and photocatalytic activity for CO_2 reduction than previously reported **[Cz-BpyRu(CO)]$_n$** without the pyrene spacer.[20] This study shows that rational molecular engineering of conjugated polymers provides a

platform for hybridising two different functional molecular catalysts for oxidation and reduction reactions by introducing specific recognition sites tailored for spatial charge separation. We believe that this strategy will provide an opportunity to achieve artificial photosynthetic reactions, such as photocatalytic CO_2 reduction coupled with water oxidation, by optimising the molecular catalyst components.

Experimental section

General procedure

^{1}H NMR (400 MHz) spectra were recorded using a JEOL ECX400 spectrometer. UV–visible absorption and diffuse reflectance spectra were recorded at a room temperature using Shimadzu UV-1800 and UV-2600i spectrophotometers, respectively. The matrix-assisted laser desorption/ionization time-of-flight mass spectrometry (MALDI-TOF-MS) were conducted using a Shimadzu MALDI-8020 mass spectrometer. Scanning electron microscopy (SEM) images were obtained using NVision 40 (Carl Zeiss–SII Nano Technology) at 1.0 kV. Photoelectron yield spectra (PYS) were measured using a Bunko Keiki BIP-KV100K instrument. The PYS measurements provided the lowest ionisation energies corresponding to the valence-band maximum potentials.[42,43] Photoelectrochemical and electrochemical measurements were conducted on a VersaSTAT4 potentiostat (AMETEK Scientific Instruments).

Material

Acetonitorile (MeCN; dehydrated, >99.5%), dimethyl sulfoxide (DMSO; >99.0%), diethyl ether (Et_2O; >99.5%), *N,N*-dimethylformamide (DMF; >99.5%), methanol (MeOH; dehydrated, >99.8%), CH_2Cl_2 (dehydrated, >99.5%), 2-propanol (>99.9%), ruthenium(III) chloride hydrate ($RuCl_3 \cdot nH_2O$; 36~44% as Ru), isoquinoline (>95.0%), potassium bicarbonate (K_2CO_3; >99.5%), tetrakis(triphenylphosphine)palladium ($Pd(PPh_3)_4$; >90.0%), boric acid (99.5%), sodium peroxodisulfate ($Na_2S_2O_8$; >97.0%), ammonium hexafluorophosphate (NH_4PF_6; >95.0%), triethanolamine (TEOA; >98.0%), p-toluenesulfonic acid (>99.0%), ethylenediamine tetra acetic acid (>99.0%), and Bis-Tris (>99.0%) were purchased from Wako Pure Chemical Industries Ltd. 2,2'–Bipyridine–6,6'-dicarboxylic acid (H_2bda; >98.0%), triethylamine (NEt_3; >99.0%), 5,5-dibromo-2,2'-bipyridine (>98.0%), 9-phenyl-2,7-bis(4,4,5,5-tetramethyl-1,3,2-dioxaborolan-2-yl)-9H-carbazole (>96.0%), 1,4-phenylenediboronic acid (>97.0%), 2,7-Bis(4,4,5,5-tetramethyl-1,3,2-dioxaborolan-2-yl)pyrene (>97.0%), and 2,7-dibromopyrene (>98.0%) were purchased from Tokyo Chemical Industry Co., Ltd. Sodium periodate ($NaIO_4$, >99.8% purity) was purchased from Sigma-Aldrich Co., LLC. The materials were used as received without further purification. $[Ru(CO)_2Cl_2]_n$ was prepared following a literature procedure.[44]

Synthesis

$[RuCl_2(DMSO)_4]$.[45] A DMSO (5 mL) solution containing $RuCl_3 \cdot nH_2O$ (500 mg, 2.4 mmol) was stirred under reflux for 30 min under a N_2 atmosphere. After cooling, iced acetone was added to the yellow solution. The precipitate obtained was filtered and washed with acetone (20 mL) and Et_2O (20 mL). Yield: 609 mg (1.3 mmol, 49%). ^{1}H NMR (400 MHz, MeOH-d_4) δ / ppm: 3.25 (m, 3H), 3.38 (m, 3H).

$[Ru(bda)(isoq)_2]$.[27] A MeOH (20 mL) solution containing *cis*-$[RuCl_2(DMSO)_4]$ (200 mg, 0.4 mmol), H_2bda (100 mg, 0.4 mmol), NEt_3 (0.3 mL) was stirred under reflux for 4 h under a N_2 atmosphere. The obtained precipitate was filtered, dissolved in MeOH (20 mL) with isoquinoline (106 mg, 0.8 mmol), and stirred under reflux for 17 h under a N_2 atmosphere. After removing the solvent, the crude product was purified by silica gel column chromatography, using CH_2Cl_2/MeOH (10:1, *v/v*) as the eluent. Yield: 72.8 mg (0.12 mmol, 29%). ^{1}H NMR (400 MHz, MeOH-d_4 (10% chloroform-*d*) with a small amount of (+) –sodium L–ascorbate) δ / ppm: 8.69 (d, *J* = 8.0 Hz, 2H), 8.66 (s, 2H), 8.06 (d, *J* = 8.0 Hz, 2H), 7.94 (t, *J* = 8.0 Hz, 2H), 7.88-7.83 (m, 5H), 7.77-7.73 (m, 2H), 7.67-7.63 (m, 4H), 7.59 (d, *J* = 6.3 Hz, 2H).

$[Ru(bda)(isoq)_2$-O-$Ru(bda)(isoq)_2(OH_2)(CH_3CN)$-O-$Ru(bda)(isoq)_2]^{2+}$.[38] A H_2O–MeCN (10:1, *v/v*; 12 mL) solution containing $[Ru(bda)(isoq)_2]$ (90.2 mg, 0.15 mmol) was stirred and added to an aqueous solution (1 mL) of $NaIO_4$ (21.4 mg, 0.10 mmol). The green solution was then treated with excess NH_4PF_6. The precipitate obtained was filtered and washed with water (15 mL). The vapour diffusion of Et_2O into a CH_3CN solution of this precipitate yielded green crystals. Yield: 51.1 mg (0.03 mmol, 53%). ^{1}H NMR (400 MHz, acetonitrile-d_3) δ / ppm: 10.42 (s, 1H), 10.16 (s, 1H), 10.03 (s, 1H), 9.32 (s, 3H), 8.96 (s, 2H), 8.48 (d, *J* = 6.3 Hz, 1H), 8.36 (d, *J* = 8.2 Hz, 1H), 8.28 (d, *J* = 8.2 Hz, 1H), 8.22 (d, *J* = 7.7 Hz, 1H), 8.15-8.02 (m, 6H), 7.92 (d, *J* = 7.7 Hz, 1H), 7.78-7.85 (m, 1H), 7.74 (d, *J* = 6.3 Hz, 2H), 7.53 (d, 1H), 7.46 (d, *J* = 6.8 Hz, 2H), 7.41 (d, *J* = 8.2 Hz, 2H), 7.35-7.27 (m, 9H), 7.21-7.14 (m, 9H), 7.12-7.06 (m, 1H), 7.00 (d, *J* = 6.3 Hz, 2H), 6.92 (d, *J* = 6.8 Hz, 2H), 6.66-6.60 (m, 2H), 6.05 (t, *J* = 5.4 Hz, 2H), 1.97 (s, 3H). UV-Vis (1% MeCN-phosphate buffer, 0.1 M, pH 7) : λ_{max} = 300 nm (4.6×10^4 $M^{-1}cm^{-1}$), 500 nm (0.6×10^4 $M^{-1}cm^{-1}$), and 690 nm (6.3×10^4 $M^{-1}cm^{-1}$).

$[Py\text{-}Bpy]_n$. A DMF–H_2O (5 : 1, *v/v*; 12 mL) solution containing 5,5'-dibromo-2,2'-bipyridine (315 mg, 1.0 mmol), 2,7-Bis(4,4,5,5-tetramethyl-1,3,2-dioxaborolan-2-yl)pyrene (454 mg, 1.0 mmol), K_2CO_3 (1040 mg, 7.5 mmol), and $Pd(PPh_3)_4$ (23.5 mg, 0.02 mmol) was stirred under reflux for 2 days under a N_2 atmosphere. The obtained precipitate was filtered and washed with water (20 mL) and MeOH (20 mL). Yield: 378 mg.

The same protocol was used for the synthesis of **$[Ph\text{-}bpy]_n$**[20] and **$[Cz\text{-}bpy]_n$**[20] using 1,4-phenylenediboronic acid and 9-phenyl-2,7-bis(4,4,5,5-tetramethyl-1,3,2-dioxaborolan-2-yl)-9H-carbazole, respectively, as starting materials instead of 2,7-bis(4,4,5,5-tetramethyl-1,3,2-dioxaborolan-2-yl)pyrene. The characterisation data are shown in Fig. S1–S2.

$[Cz\text{-}Py/Bpy]_n$. A DMF–H_2O (5 : 1, *v/v*; 12 mL) solution containing 5,5'-dibromo-2,2'-bipyridine (157 mg, 0.45 mmol), 2,7-dibromopyrene (18.0 mg, 0.05 mmol), 9-phenyl-2,7-bis(4,4,5,5-tetramethyl-1,3,2-dioxaborolan-2-yl)-9H-carbazole (248 mg, 0.50 mmol), K_2CO_3 (520 mg, 3.8 mmol), and $Pd(PPh_3)_4$ (11.8 mg, 0.01 mmol) was stirred under reflux for 2 days under N_2 atmosphere. The obtained precipitate was filtered and washed with water (20 mL) and MeOH (20 mL). Yield 190 mg.

[Cz/Py-Bpy]$_n$. A DMF–H_2O (5 : 1, *v/v*; 12 mL) solution containing 5,5'-dibromo-2,2'-bipyridine (141.7 mg, 0.5 mmol), 2,7-Bis(4,4,5,5-tetramethyl-1,3,2-dioxaborolan-2-yl)pyrene (22.7 mg, 0.05 mmol), 9-phenyl-2,7-bis(4,4,5,5-tetramethyl-1,3,2-dioxaborolan-2-yl)-9H-carbazole (223 mg, 0.45 mmol), K_2CO_3 (520 mg, 3.8 mmol), and $Pd(PPh_3)_4$ (11.8 mg, 0.01 mmol) was stirred under reflux for 2 days under a N_2 atmosphere. The obtained precipitate was filtered and washed with water (20 mL) and MeOH (20 mL). Yield: 179.9 mg.

[Ru(bda)(isoq)$_2$]/[X-Bpy]$_n$. A dispersion of **[X-Bpy]$_n$** (X = Ph, Py, Cz or Py-Cz) or **[Cz/Py-Bpy]$_n$** in H_2O-MeCN (9 : 1, *v/v*; 50 mL) containing various concentrations of [Ru(bda)(isoq)$_2$] was placed in a Pyrex Erlenmeyer flask. After stirring for 3 h, the solution was filtered through a filter (Omnipore 0.22 μm PTFE membrane). The amount adsorbed was calculated from the difference between the concentrations of [Ru(bda)(isoq)$_2$] in solution before and after adsorption, which were estimated from the absorbance at 304 nm.

[Cz-Py/BpyRu(CO)]$_n$. A MeOH dispersion (5 mL) containing $[Ru(CO)_2Cl_2]_n$ (22.8 mg, 0.1 mmol) and **[Cz-Py/Bpy]$_n$** (39.2 mg, 0.1 mmol) was refluxed through stirring for 17 h under a N_2 atmosphere. After refluxing, the obtained precipitate was filtered and washed with MeOH (20 mL). Yield: 49.7 mg. FT-IR (ATR): ν_{CO} = 2055, 1981 cm^{-1}.

The same protocol was applied for the synthesis of **[Cz-BpyRu(CO)]$_n$**.

Time-resolved microwave conductivity measurement

Time-resolved microwave conductivity experiments were performed using a third harmonic generator (THG; 355 nm) of an Nd:YAG laser (Continuum Inc., Surelite II, 5–8 ns pulse duration, 10 Hz) as the excitation source (9.1×10^{15} photons per cm^2 per pulse) and X-band microwave (~9.1 GHz) as the probe. Photoconductivity $\Delta\sigma$ was obtained using Eqn. (1):

$$\Delta\sigma = \Delta P_r/(AP_r) \quad (1)$$

where ΔP_r, A, and P_r are the transient power changes in the reflected microwave power, the sensitivity factor, and the reflected microwave power, respectively. The transient photoconductivity $\Delta\sigma$ was converted to the product of the quantum yield (ϕ) and sum of the charge carrier mobilities $\Sigma\mu$ using Eqn. (2) and (3):

$$\Sigma\mu = \mu^+ + \mu^- \quad (2)$$

$$\phi\Sigma\mu = \Delta\sigma/(eI_0F_{light}) \quad (3)$$

where e and F_{light} are the unit charge of a single electron and the correction (or filling) factor, respectively. The experiments were conducted in air at room temperature (298 K).

X-ray absorption fine structure spectroscopy measurement

X-ray absorption fine structure spectroscopy (XAFS) measurements were performed at the PF-AR NW10A beamline of the Photon Factory (High Energy Accelerator Research Organization, Tsukuba, Japan). The X-ray energy was varied by using a Si(311) double-crystal monochromator. The reference samples were diluted in boron nitride, compressed to form pellets, and measured in the transmission mode. [Ru(bda)(isoq)$_2$]-loaded samples were measured in the fluorescence mode using a multichannel solid-state detector.

Photoelectrochemical and electrochemical measurements

A series of photoelectrodes was prepared on conductive fluorine doped tin oxide (FTO) glass using the squeegee method. A slurry of the photocatalyst powder in 2-propanol was pasted onto the FTO glass. The coated area was fixed at dimensions approximately 1.5 × 3.5 cm, wherein 1 mg of the photocatalyst was included.

Photoelectrochemical measurements were performed in a boric acid buffer (0.1 M) under an Ar atmosphere. The photocatalyst electrode, Ag/AgCl reference electrode, and Pt wire counter electrode were connected to a potentiostat. The photocatalyst electrodes were irradiated with visible light ($400 < \lambda < 800$ nm) using a Xe lamp (Cermax, 300 W) fitted with a CM-1 cold mirror and an L-42 cutoff filter at an applied potential of 1.0 V vs. Ag/AgCl while chronoamperometry was recorded.

Photocatalytic reactions

The photocatalytic water oxidation reactions were conducted using a glass closed gas circulation system. A suspension of the photocatalyst (50 mg) in 50 mL of boric acid buffer (20 mM, pH 7.0, adjusted with NaOH) containing $Na_2S_2O_8$ (10 mM) was stirred in a Pyrex glass vessel. The reaction suspension was evacuated and purged with Ar before photoirradiation. A Xe lamp (Cermax, 300 W) was used as the light source in combination with a CM-1 cold mirror and an L-42 cutoff filter for illumination with visible light ($400 < \lambda < 800$ nm). The evolved gases were analysed using a gas chromatography (GC-8A, Shimadzu, TCD detector, MS 5A column, and Ar carrier) connected directly to the closed gas circulation system.

Photocatalytic CO_2 reduction reactions were conducted using a merry-go-round system. A suspension of the photocatalyst (2 mg) in 2 mL of an aqueous sodium ascorbate solution (10 mM) containing Na_2CO_3 (50 mM) was placed in a Pyrex test tube (inner diameter: 10 mm; volume: 8.4 mL). The reaction suspension was purged by CO_2 bubbling (20 min) and sealed using a rubber septum prior to photoirradiation. The sample tube was placed in an LED merry-go-round reactor (Iris-MG-S, Cell System Inc.) and irradiated with visible light ($400 < \lambda < 700$ nm) while stirring. The gaseous products, CO and H_2 were analysed using a GL Science GC 3210 gas chromatograph (MS-5A column, Ar carrier) combined with a TCD detector. The formate produced in the liquid phase was analysed using a Shimadzu LC-20AT HPLC system equipped with two Shimadzu Shim-pack FAST-OA columns (100 × 7.8 mm) and a Shimadzu CDD-10A conductivity detector. An aqueous solution containing p-toluenesulfonic acid (0.95 g L^{-1}) was used as the eluent at a flow rate of 0.8 mL min^{-1} (column temperature: 313 K). After column separation, the eluent was mixed with an aqueous solution containing p-toluenesulfonic acid (0.95 g L^{-1}), ethylenediaminetetraacetic acid (0.03 g L^{-1}), and Bis–Tris (4.18 g L^{-1}). The external quantum efficiencies (EQE) of photocatalytic reactions were determined on the basis of Eqn (4):

$$\text{EQE} = \frac{n \times \text{Amount of product (mol)}}{\text{Inputted photon (einstein)}} (4)$$

where n indicates the numbers of electrons required to generate one molecule of the product (*i.e.*, 4 for O_2 generation by water oxidation and 2 for formate formation by CO_2 reduction).

Computational details

Density functional theory (DFT)[46] calculations were performed using the DMol^3 software[47] in the Materials Studio suite of programs.[48] The molecular orbitals of each compound were obtained using the generalised gradient approximation (GGA) level of theory with the Perdew–Burke–Ernzerhof (PBE) semi-local exchange-correlation functional.[49] Core elements were treated with all-electron pseudopotentials and the DNP basis set using basis set file 4.4.

Conflicts of interest

There are no conflicts to declare.

Acknowledgements

This work was supported by JST PRESTO grant JPMJPR20T5 (Controlled Reaction), JSPS Grant-in-Aid for Transformative Research Areas (B) "Concerto Photocatalysis" (Grant Numbers JP23H03832 and JP23H03830), as well as JSPS KAKENHI Grants JP20H00398 and JP24K01603. The authors would like to acknowledge Dr. Tomoki Kanazawa and Dr. Rie Haruki, High Energy Accelerator Research Organization (KEK), for helping XAFS measurements.

References

1 Y. Ma, X. Wang, Y. Jia, X. Chen, H. Han and C. Li, *Chem. Rev.*, 2014, **114**, 9987–10043.
2 S. N. Habisreutinger, L. Schmidt-Mende and J. K. Stolarczyk, *Angew. Chem. Int. Ed.*, 2013, **52**, 7372–7408.
3 S. Lin, H. Huang, T. Ma and Y. Zhang, *Adv. Sci.*, 2021, **8**, 2002458.
4 A. J. Morris, G. J. Meyer and E. Fujita, *Acc. Chem. Res.*, 2009, **42**, 1983–1994.
5 Y. Yamazaki, H. Takeda and O. Ishitani, *J. Photochem. Photobiol., C*, 2015, **25**, 106–137.
6 J. D. Blakemore, R. H. Crabtree and G. W. Brudvig, *Chem. Rev.*, 2015, **115**, 12974–13005.
7 T. Morikawa, S. Sato, K. Sekizawa, Tomiko. M. Suzuki and T. Arai, *Acc. Chem. Res.*, 2022, **55**, 933–943.
8 A. Nakada, H. Kumagai, M. Robert, O. Ishitani and K. Maeda, *Acc. Mater. Res.*, 2021, **2**, 458–470.
9 B. A. Pinaud, J. D. Benck, L. C. Seitz, A. J. Forman, Z. Chen, T. G. Deutsch, B. D. James, K. N. Baum, G. N. Baum, S. Ardo, H. Wang, E. Millere and T. F. Jaramillo, *Energy Environ. Sci.*, *2013*, **6**, 1983–2002.
10 H. Nishiyama, T. Yamada, M. Nakabayashi, Y. Maehara, M. Yamaguchi, Y. Kuromiya, Y. Nagatsuma, H. Tokudome, S. Akiyama, T. Watanabe, R. Narushima, S. Okunaka, N. Shibata, T. Takata, T. Hisatomi and K. Domen, *Nature*, *2021*, **598**, 304–307.
11 G. Sahara, H. Kumagai, K. Maeda, N. Kaeffer, V. Artero, M. Higashi, R. Abe and O. Ishitani, *J. Am. Chem. Soc.*, 2016, **138**, 14152–14158.
12 S. Yoshino, T. Takayama, Y. Yamaguchi, A. Iwase and A. Kudo, *Acc. Chem. Res.*, 2022, **55**, 966–977.
13 H. Kumagai, Y. Tamaki and O. Ishitani, *Acc. Chem. Res.*, 2022, **55**, 978–990.
14 Y. Wang, A. Vogel, M. Sachs, R. S. Sprick, L. Wilbraham, S. J. A. Moniz, R. Godin, M. A. Zwijnenburg, J. R. Durrant, A. I. Cooper and J. Tang, *Nat. Energy*, 2019, **4**, 746–760.
15 Z.-P. Yu, K. Yan, W. Ullah, H. Chen and C.-Z. Li, *ACS Appl. Polym. Mater.*, 2021, **3**, 60–92.
16 T. Banerjee, F. Podjaski, J. Kröger, B. P. Biswal and B. V. Lotsch, *Nat. Rev. Mater.*, 2021, **6**, 168–190.
17 Y. Li, *Acc. Chem. Res.*, 2012, **45**, 723–733.
18 A. S. Maier, C. Thomas, M. Kränzlein, T. M. Pehl and B. Rieger, *Macromolecules*, 2022, **55**, 7039–7048.
19 F. Adams, M. Pschenitza and B. Rieger, *ChemCatChem*, 2018, **10**, 4309–4316.
20 A. Nakada, R. Miyakawa, R. Itagaki, K. Kato, C. Takashima, A. Saeki, A. Yamakata, R. Abe, H. Nakai and H.-C. Chang, *J. Mater. Chem. A*, 2022, **10**, 19821–19828.
21 R. S. Sprick, Z. Chen, A. J. Cowan, Y. Bai, C. M. Aitchison, Y. Fang, M. A. Zwijnenburg, A. I. Cooper and X. Wang, *Angew. Chem. Int. Ed.*, 2020, **59**, 18695–18700.
22 Y. Bai, C. Li, L. Liu, Y. Yamaguchi, M. Bahri, H. Yang, A. Gardner, M. A. Zwijnenburg, N. D. Browning, A. J. Cowan, A. Kudo, A. I. Cooper and R. S. Sprick, *Angew. Chem. Int. Ed.*, 2022, **61**, e202201299.
23 J. Bi, W. Fang, L. Li, J. Wang, S. Liang, Y. He, M. Liu and L. Wu, *Macromol. Rapid Commun.*, 2015, **36**, 1799–1805.
24 S. Qiao, M. Di, J.-X. Jiang and B.-H. Han, *EnergyChem*, 2022, **4**, 100094.
25 J. Yang, D. Wang, H. Han and C. Li, *Acc. Chem. Res.*, 2013, **46**, 1900–1909.
26 L. Duan, F. Bozoglian, S. Mandal, B. Stewart, T. Privalov, A. Llobet and L. Sun, *Nature Chem.*, 2012, **4**, 418–423.
27 L. Wang, L. Duan, Y. Wang, M. S. G. Ahlquist and L. Sun, *Chem. Commun.*, 2014, **50**, 12947–12950.
28 L. Duan, Y. Xu, P. Zhang, M. Wang and L. Sun, *Inorg. Chem.*, 2010, **49**, 209–215.
29 F. Li, Y. Jiang, B. Zhang, F. Huang, Y. Gao and L. Sun, *Angew. Chem. Int. Ed.*, 2012, **51**, 2417–2420.
30 L. Li, L. Duan, Y. Xu, M. Gorlov, A. Hagfeldt and L. Sun, *Chem. Commun.*, 2010, **46**, 7307–7309.
31 D. Eder and A. H. Windle, *Adv. Mater.*, 2008, **20**, 1787–1793.
32 F. Liang, J. Zhang, Z. Hu, C. Ma, W. Ni, Y. Zhang and S. Zhang, *ACS Appl. Mater. Interfaces*, 2021, **13**, 25523–25532.
33 M. V. Sheridan, B. D. Sherman, Z. Fang, K.-R. Wee, M. K. Coggins and T. J. Meyer, *ACS Catal.*, 2015, **5**, 4404–4409.
34 I. Botiz, R. D. Schaller, R. Verduzco and S. B. Darling, *J. Phys. Chem. C*, 2011, **115**, 9260–9266.
35 Lan Z.-A., Ren W., Zhang Y. and Wang X., *Appl. Catal. B*, 2019, **245**, 596–603.
36 K. Maeda, R. Abe and K. Domen, *J. Phys. Chem. C*, 2011, **115**, 3057–3064.
37 H. Suzuki, S. Nitta, O. Tomita, M. Higashi and R. Abe, *ACS Catal.*, 2017, **7**, 4336–4343.
38 B. Zhang, F. Li, R. Zhang, C. Ma, L. Chen and L. Sun, *Chem. Commun.*, 2016, **52**, 8619–8622.
39 A. Nakada, T. Nakashima, K. Sekizawa, K. Maeda and O. Ishitani, *Chem. Sci.*, 2016, **7**, 4364–4371.
40 G. Zhang, S. Zang and X. Wang, *ACS Catal.*, *2015*, **9**, 941–947.
41 R. Kuriki, H. Matsunaga, T. Nakashima, K. Wada, A. Yamakata, O. Ishitani and K. Maeda, *J. Am. Chem. Soc.*, *2016*, **138**, 5159–5170.
42 Y. Nakayama, S. Machida, D. Tsunami, Y. Kimura, M. Niwano, Y. Noguchi and H. Ishii, *Appl. Phys. Lett.*, 2008, **92**, 153306.

43 H. Suzuki, H. Kunioku, M. Higashi, O. Tomita, D. Kato, H. Kageyama and R. Abe, *Chem. Mater.*, 2018, **30**, 5862–5869.
44 P. A. Anderson, G. B. Deacon, K. H. Haarmann, F. R. Keene, T. J. Meyer, D. A. Reitsma, B. W. Skelton, G. F. Strouse and N. C. Thomas, *Inorg. Chem.*, 1995, **34**, 6145–6157.
45 I. P. Evans, A. Spencer and G. Wilkinson, *J. Chem. Soc., Dalton Trans.*, 1973, 204–209.
46 W. Kohn and L. J. Sham, *Phys. Rev.*, 1965, **140**, A1133–A1138.
47 B. Delley, *J. Chem. Phys.*, 1990, **92**, 508–517.
48 Materials Studio; BIOVIA: San Diego, CA, USA, 2018.
49 J. P. Perdew, K. Burke and M. Ernzerhof, *Phys. Rev. Lett.*, 1996, **77**, 3865–3868.

Data availability statements

The data supporting this article have been included as part of the Supplementary Information.